J. Fluid Mech. (1968), *vol.* 34, *part* 3, *pp.* 551–564
Printed in Great Britain

A theoretical investigation of disturbance amplification in external laminar natural convection

By R. P. DRING
N.S.F. Trainee, Cornell University

AND B. GEBHART
Professor of Mechanical Engineering Cornell University

(Received 5 February 1968)

The nature of instability and disturbance amplification in the laminar natural convection boundary layer over a vertical flat surface with uniform heat flux has been theoretically investigated. The coupled Orr–Sommerfeld equation has been numerically integrated for a Prandtl number of 6·7, with the boundary condition that the disturbance heat flux be zero at the surface. The spatial amplification characteristics of disturbances convected downstream were analyzed, and constant amplification rate contours were determined. The relative amplification has been calculated from these contours and is presented in the form of amplitude ratio contours. An important feature of these results is that the low frequency disturbances, which become unstable first, amplify very slowly and also have wavelengths which are much longer than the distance to the leading edge. The higher frequency, shorter wavelength, disturbances amplify much faster and are, therefore, presumed to be the dominant ones in stability considerations. The nature of the velocity and temperature amplitudes and phase profiles across the boundary layer has also been examined.

1. Introduction

Progress in the study of stability, of wave amplification toward transition, and of turbulence in external natural convection flows has lagged behind similar studies in forced flow .This is at least partially a result of the greater complexity of natural convection flows. The results in forced flow have often, however, pointed out the most promising theoretical and experimental approaches to the natural convection problem.

The first analytical investigation of external natural convection laminar instability was a study by Plapp (1957). The coupling of the momentum and energy disturbance equations, through the temperature dependent body force term, was demonstrated. Several early attempts at solving these equations were very approximate and restricted to considerations of the uncoupled momentum equation only (i.e. the coupling term was neglected).

Nachtsheim (1963) presented the first complete solutions of the coupled disturbance equations. These were obtained by numerically integrating the

equations of Plapp (1957) across the boundary layer. In addition to some calculations without coupling, the full equations were solved for air ($Pr = 0{\cdot}733$) and for water ($Pr = 6{\cdot}7$), for flow over a vertical isothermal surface. The temperature disturbance was taken as zero at the surface. The inclusion of coupling had a significant effect on the location and shape of the neutral curves.

Polymeropoulos & Gebhart (1967) reported the first critical experimental study of incipient laminar instability in external natural convection flows. Employing techniques found successful in force flows, and a 20 cm Mach–Zehnder interferometer, many of the theoretical results of Nachtsheim (1963) were verified.

In a recent theoretical and experimental investigation, Knowles (1967) examined the coupled equations numerically for the flow over a vertical uniform flux surface. He considered a range of Prandtl numbers from 0·733 to 6·9 and showed the effect of the nature of the boundary condition imposed on the temperature disturbance at the surface.

The present work relies heavily on the results of these investigators, and in many ways it is an extension of the work of Knowles & Gebhart (1968).

2. Theory

The laminar flow (i.e. the base flow) whose stability properties are under investigation here, is the natural convection flow about a vertical flat surface. This work was intended for eventual comparison with experimental data taken in the natural convection flow of a liquid ($Pr = 6{\cdot}7$) about a thin vertical, electrically heated foil. The foil generates a uniform heat flux over its area, so the base flow was taken as the flow over a uniform flux surface.

The flow is laminar near the leading edge and for some distance up the surface. Farther up the surface the flow will undergo transition to turbulence. It is the stability of the laminar flow preceeding transition that is under investigation. The flow is said to be stable at a location if a disturbance to the laminar flow field tends to dampen out as it is convected past that location. The flow is said to be neutrally stable if the disturbance amplitude does not change, and unstable if it grows. As expected, this behaviour is a strong function of the frequency of the disturbance.

The base flow is a function of x (distance from the leading edge) and y (distance normal to the plate). A solution similar to those presented by Sparrow & Gregg (1956) was used for the uniform heat flux base flow. The disturbances are taken to be functions of x, y and t (time). Natural convection stability considerations are more complex than those of forced flow, since the energy equation is coupled to the momentum equation through the body force term. Both velocity and temperature disturbances must be considered simultaneously. The disturbance stream function and temperature are assumed to have the form

$$\tilde{\psi}(\tilde{x}, \tilde{y}, \tilde{t}) = \tilde{\phi}(\tilde{y}) \exp\{i(\tilde{\alpha}\tilde{x} - \tilde{\beta}\tilde{t})\}, \tag{1}$$

$$\tilde{\theta}(\tilde{x}, \tilde{y}, \tilde{t}) = \tilde{s}(\tilde{y}) \exp\{i(\tilde{\alpha}\tilde{x} - \tilde{\beta}\tilde{t})\}. \tag{2}$$

For $\tilde{\alpha}$ (wave-number) and $\tilde{\beta}$ (frequency) complex, these functions describe a travelling wave disturbance in the flow. The amplitude and phase are functions of the distance normal to the surface ($\tilde{y}$).

The momentum and energy equations are linearized with these two disturbance quantities. The terms containing derivatives of the base flow quantities with respect to x are neglected (i.e. the base flow in the disturbance equations is assumed to be a function of y only). The results of this one-dimensional analysis will be used to predict the behaviour of a disturbance in a two-dimensional base flow. This is not unreasonable since derivatives of the base flow quantities with respect to x are much smaller than derivatives with respect to y.

The equations are non-dimensionalized using the characteristic length ($\tilde{\delta}_c = 5\tilde{x}/G^*$), velocity ($\tilde{U}_c = \nu G^{*2}/5\tilde{x}$) and temperature ($\tilde{T}_c = 5q''\tilde{x}/kG^*$) for a uniform flux base flow where $G^* = 5(Gr^*/5)^{\frac{1}{5}}$ and $Gr^* = (g\beta_T q''\tilde{x}^4/k\nu^2)$. Except for the sign of $\tilde{T}_c$, these are the same characteristic quantities used by Polymeropoulos & Gebhart (1966) in their study of the stability of this type of base flow. The result is the coupled Orr–Sommerfeld equation:

$$\left(U - \frac{\beta}{\alpha}\right)(\phi'' - \alpha^2\phi) - \phi U'' + \frac{i}{\alpha G^*}(\phi^{\mathrm{iv}} - 2\alpha^2\phi'' + \alpha^4\phi + s') = 0, \tag{3}$$

$$\left(U - \frac{\beta}{\alpha}\right)s - \phi T' + \frac{i}{\alpha G^* Pr}(s'' - \alpha^2 s) = 0, \tag{4}$$

where U and T are the dimensionless base flow velocity and temperature profiles respectively. All quantities in these equations are dimensionless and primes ($'$) denote derivatives with respect to ($\eta = \tilde{y}/\tilde{\delta}_c$). These are analogous to those equations originally derived by Plapp (1957). Inclusion of temperature disturbances has made this a sixth-order set of equations as compared to a fourth-order set in the uncoupled and forced flow cases.

The normal and tangential components of disturbance velocity (i.e. ϕ and ϕ') must go to zero at the surface and far from it. The disturbance temperature must also go to zero far from the surface. It has been shown by Knowles & Gebhart (1968) that at the surface the boundary condition on the disturbance temperature is

$$s(0) = \frac{i}{Q^{*2}\beta}s'(0), \tag{5}$$

where $Q^* = (Pr/5)[(C_v l)_s/(C_v\tilde{x})_f]$. This is the result of a heat balance at the surface. It relates the time rate of change of the energy stored in the surface, due to thermal capacity, to the disturbance heat flux in the fluid at the surface. This boundary condition results from a thermal capacity coupling between the vertical element and the fluid. This is a large effect and is important in many practical natural convection configurations. The nature and effect of this boundary condition is discussed in detail by Knowles & Gebhart (1968).

This boundary condition can be rewritten as

$$s(0) = \frac{i}{QG^{*\frac{3}{4}}\beta}s'(0), \tag{6}$$

where $Q = [Pr[(C_v)_s/(C_v)_f](g\beta_T q'' l^4/k\nu^2)^{\frac{1}{4}}]$. Written in this form the new parameter, Q, unlike Q^*, is independent of location (i.e. it is not a function of x). Solutions could be determined for any value of Q. The two extreme cases of this boundary condition are $s(0) = 0$ and $s'(0) = 0$ (when $QG^{*\frac{1}{4}}\beta$ is large and small respectively). All physical situations are between these two extreme conditions. These extremes, however, have the advantage that they are independent of G^* and β. The $s'(0) = 0$ boundary condition was chosen for this present work because both Q and G^* are relatively small for thin elements in liquids. Q is small because of the low heat capacity of the thin metal foils used to generate the flow and G^* is relatively small because consideration is being given to the earlier stages of disturbance amplification. The $s(0) = 0$ boundary condition applies when Q and G^* are large. Q would be large for a surface with a large heat capacity.

The problem, as stated to this point, has been investigated by Knowles & Gebhart (1968). Among other things, they located one point on the neutral curve for a Prandtl number of 6·7. At a Prandtl number of 6·9, they located the lower branch of the neutral curve, and the upper branch out to $G^* = 65$. All their investigations were confined to studies of neutral curves. The subject of the present paper is an improved method of solution of the disturbance equations. By this improved method the solutions are extended into the damped and amplified regions and to larger values of G^*.

An asymptotic solution like that used by Nachtsheim (1963) is needed in the region outside the boundary layer. In that region the base flow quantities in the Orr–Sommerfeld equation (i.e. U, U'' and T') go to zero. In order to obtain an asymptotic solution these quantities are set equal to zero in the disturbance equations. The result is two ordinary differential equations (with constant coefficients) for the amplitude functions:

$$\phi'''' - (a^2+b^2)\phi'' + (a^2b^2)\phi + s' = 0, \tag{7}$$

$$s'' - c^2 s = 0, \tag{8}$$

where $$a = \alpha, \quad b = (\alpha^2 - i\beta G^* Pr)^{\frac{1}{2}}, \quad c = (\alpha^2 - i\beta G^* Pr)^{\frac{1}{2}}.$$

These asymptotic equations have the general solutions (when $Pr \neq 1$)

$$\phi = c_1 e^{a\eta} + c_2 e^{-a\eta} + c_3 e^{b\eta} + c_4 e^{-b\eta} + c_5 e^{c\eta} + c_6 e^{-c\eta}, \tag{9}$$

$$s = \left(\frac{-c_5}{c}\right)(c^2-a^2)(c^2-b^2)\, e^{c\eta} + \left(\frac{c_6}{c}\right)(c^2-a^2)(c^2-b^2)\, e^{-c\eta}. \tag{10}$$

Since both ϕ and s go to zero as η goes to infinity, the coefficients of the terms whose exponents have positive real parts should be identically zero. Depending on the manner in which the numbers b and c are calculated, this means that either c_1, c_3 and c_5, or c_1, c_4 and c_6 must be zero. The results of the square-root algorithm used to calculate b and c depend on whether complex numbers with negative imaginary parts are considered to have arguments between π and 2π or between 0 and $-\pi$.

The general method of solution is to integrate numerically the full equations (3) and (4) across the boundary layer, simultaneously satisfying the asymptotic solution at the outer edge and the boundary conditions at the surface. The

choice must now be made as to the direction of integration. If the equations are integrated going away from the surface, the solutions must be matched with the asymptotic solution at the edge of the boundary layer. This method was used by Nachtsheim (1963) and Knowles & Gebhart (1968). The starting values at the surface (and the other eigenvalues) are adjusted until the coefficients of the terms with positive real parts in their exponents (c_1, c_3 and c_5 or c_1, c_4 and c_6) become small. This method has within it the shortcoming that no matter how precisely one knows the starting values, the solutions will eventually increase without limit if carried to large enough values of η even though the coefficients of the terms with positive real parts in their exponents are extremely small. This practical difficulty usually arises at large values of G^* because of the strong dependence of b and c on G^*.

This problem can be avoided entirely by integrating from the edge of the boundary layer in, toward the surface (refer to Kaplan (1964)). In this procedure the integrations are started with the asymptotic solution using only the terms with negative real parts in their exponents. The coefficients of the exponentials (and the other eigenvalues) are adjusted until the values of ϕ, ϕ' and s' become *small* at the surface. In addition to being more stable, this method offers certain computational advantages. When integrating away from the surface, all of the starting values are known, or guessed, at the surface. A Runge–Kutta integrator is generally used to start the integration. When enough back-points have been calculated, a faster integrator (such as Adams method) is used. When integrating in, no such change is necessary since the asymptotic solution can provide as many back-points as is necessary to start the integrator. For these reasons, all of the integrations in this present work were done going toward the surface.

For this problem the outer edge of the boundary layer was taken at $\eta = 5$, and a step size of 0·10 was used. The results of this programme, where comparable, were in excellent agreement with those of Knowles (1967), where the effect of step size and boundary-layer thickness were thoroughly investigated. Since it was intended to use this programme for calculations at a large number of points on the stability plane, it was an economic necessity that the calculation at each point be very fast. Since calculation time is roughly proportional to the boundary-layer thickness used, the slight loss of accuracy involved with using a thickness of 5 was considered worth the large reduction in computer time needed. Using a thickness of 6 instead of 5 would have required about 20 % more computer time for the same results.

The eigenvalues of the solution were chosen as the real part of the wave-number (α_r), the real part of the frequency (β_r) and the coefficients of the exponentials in the asymptotic solution (c_4 and c_6). Since the equations are linear, and the boundary conditions are homogeneous, ϕ was set equal to one at $\eta = 5$. This fixed c_2, once the other two coefficients were known. The square-root algorithm used in this work considered complex numbers with negative imaginary parts to have arguments between 0 and $-\pi$. As a result of this, c_1, c_3 and c_5 were taken to be identically zero. This left the distance amplification rate (α_i), the time amplification rate (β_i) and G^* as input parameters. This choice of eigenvalues allows one to choose a contour of constant amplification rate and to march

along it by changing G^*. The solution at each G^* will be a solution on the contour. β_i was always taken to be zero, so β is a real number. This is in agreement with the experimental situation where a wave is introduced at some location and amplifies at constant frequency ($\tilde{f}$) as it travels downstream. The amplification is with distance, as indicated by α_i. The amplitude at a particular location is time-steady. Under these conditions the neutral curve and amplification rate contours were located.

A fourth-order Adams predictor-corrector integrator was used. The asymptotic solution provided the values of the functions and of the derivatives at the edge of the boundary layer, and at three other back-points. The equations were integrated toward the surface to give ϕ, ϕ' and s' at $\eta = 0$. Corrections were then made on the eigenvalues according to the Newton–Raphson technique employed by Nachtsheim (1963). This method required the integration of correction equations across the boundary layer. These were started and integrated in the same manner as the Orr–Sommerfeld equation. In all, a total of sixty first-order, real equations were integrated across the fifty points in the boundary layer with each iteration.

Two numbers were used as indicators of convergence in the Newton–Raphson iterations. The first was the sum of the absolute values of the relative changes of of the six eigenvalues. It was demanded that this indicator be less than 10^{-6}. The second indicator was the sum of the absolute values of the real and imaginary parts of ϕ, ϕ' and s' at $\eta = 0$. This was actually a relative indicator since ϕ was always equal to one at the edge of the boundary layer. During the final stages of convergence, the second indicator usually lagged behind the first. This lag was the eventual cause of terminating calculations at large values of G^*.

It was intended to solve the Orr–Sommerfeld equation at a large number of points from the 'critical' G^* (i.e. the minimum G^* at which the flow is unstable) up to a G^* of 300. The simplest way to do this is to march in relatively small steps from points where convergence has already been achieved. One method of doing this is to change one of the parameters (G^* for example) slightly at a point where the eigenvalues are known. If the change is small enough, the eigenvalues would be expected to change only slightly, and the Newton–Raphson iterations can then be used until convergence is achieved at the new point. This method of marching would be improved if a better first guess had been used for the eigenvalues at the new point. This improvement would be seen in a faster convergence and the larger step sizes possible. A number of extrapolation procedures were tried, but a simple least-squares straight line fit was chosen. A line was fitted through each eigenvalue at four points where convergence had been achieved. When beginning a march, four points were calculated by marching with small steps and without an extrapolator. The extrapolator was then used with these four back-points and a much larger step size. As each new point was calculated, the oldest point was dropped, and the least-squares lines were calculated for a new set of points. The programme was marched in α_i with G^* held constant, and in G^* with α_i held constant. The marching procedure worked well over the entire (β, G^*)-plane except where the marching parameter (α_i or G^*) went through an extreme. For example, G^* goes through a minimum at the nose of the neutral

curve. When such an extreme occurs, the eigenvalues cannot be accurately predicted by the extrapolator because they vary rapidly with small changes in the marching parameter. In such situations graphical extrapolation, i.e. curve plotting, was found to be best. Using these various procedures, the amplification rate contours were located on the β–G^* diagram (figure 1).

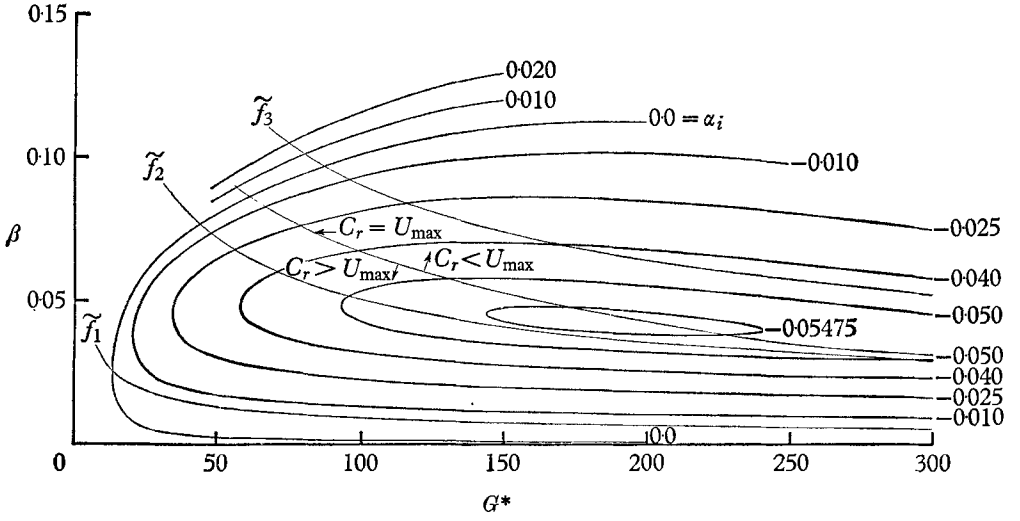

FIGURE 1. Distance amplification rate (α_i) contours plotted on β–G^* co-ordinates.

As mentioned, it became increasingly difficult to satisfy the boundary conditions at the surface at large values of G^* and particularly when β was also large, i.e. on the upper branches of the contours. As the corrections to the eigenvalues became smaller, the values of ϕ, ϕ' and s' at $\eta = 0$ also decreased, but not as fast. Eventually, the eigenvalue corrections were in the last few significant figures, and if the values of ϕ, ϕ' and s' at $\eta = 0$ were not small enough, the alternative was to go to double precision arithmetic. This slows down the calculation rate tremendously. This was the cause of the termination of calculation and the reason why the upper branches of the $\alpha_1 = 0$ and $-0{\cdot}010$ curves are not complete. By using double precision arithmetic Knowles (1967) found that the eigenfunctions were improved, i.e. the boundary conditions were satisfied more accurately. The eigenvalues, however, only underwent changes in the last few significant figures. Thus, even though the boundary conditions on the eigenfunctions at $\eta = 0$ could not be met satisfactorily with single precision, the eigenvalues could be determined with acceptable accuracy.

3. Results

Two distinct types of information were produced by the programme, the eigenvalues and the eigenfunctions. As mentioned, the eigenvalues were known to at least six significant figures. The eigenvalue information is shown in figure 1 in the form of a plot of β versus G^*. β equals β_r because β_i was taken to be identi-

cally zero. G^* is analogous to the Reynolds number (based on boundary-layer thickness) in the forced flow case, since both occur in the same way in the Orr–Sommerfeld equation. This Reynolds number is proportional to the square-root of the distance from the leading edge ($\tilde{x}^{\frac{1}{2}}$), but G^* is proportional to $\tilde{x}^{\frac{1}{8}}$. The data forms contours of constant distance amplification rate (α_i). The relative amplitude growth rate is proportional to $-\alpha_i$. From this value one can calculate the rate at which a disturbance amplifies (or decays) as it is convected downstream. The neutral curve ($\alpha_i = 0$) goes through a critical (minimum) G^* of 13·5 (at $\beta = 0{\cdot}0255$) and has a maximum β of 0·1121 at $G^* = 189$. The calculation of the neutral curve and the $\alpha_i = -0{\cdot}010$ contour were stopped at $G^* = 200$ and 250 respectively because of the difficulties with the eigenfunctions, although they probably could have been continued with little loss of accuracy, given sufficient machine time.

An investigation was made into the possibility of amplification rate contour closure. The contour for a high amplification rate ($\alpha_i = -0{\cdot}05475$) was examined. It was shown that this contour does close. Apparently lower α_i contours also close at higher values of G^*. However, it is still unknown as to whether the neutral curve closes, i.e. whether or not the upper branch has a non-zero asymptote.

As a disturbance is convected downstream its amplitude changes as a result of two effects. The base flow velocity and temperature increase in the downstream direction, and this increases the disturbance amplitude. This type of disturbance growth is accounted for by the non-dimensionalization. $\tilde{U}_e$ is proportional to $\tilde{x}^{\frac{1}{8}}$, and $\tilde{T}_e$ is proportional to $\tilde{x}^{\frac{1}{8}}$. There is, however, a second mechanism for disturbance decay and growth in the flow, and it is characterized by the Orr–Sommerfeld equation. It predicts the decay and amplification of the non-dimensionalized amplitudes. When a disturbance is neutrally stable at a point, its non-dimensionalized amplitude is neither increasing nor decreasing, but its actual (dimensional) amplitude is increasing in proportion to the increase in the base flow quantities.

It is the growth of the non-dimensionalized amplitude as the disturbance is convected downstream which leads to transition and turbulence (refer to Smith (1956)). As a disturbance travels from $\tilde{x}_1$ to $\tilde{x}_2$, its non-dimensionalized amplitude ratio for the two locations ((A_2/A_1), where A_1 and A_2 are the non-dimensionalized disturbance amplitudes at $\tilde{x}_1$ and $\tilde{x}_2$ respectively) is given by the following expression

$$(A_2/A_1) = \exp\left\{-\int_{\tilde{x}_1}^{\tilde{x}_2} \tilde{\alpha}_i d\tilde{x}\right\}. \tag{11}$$

The integral can be non-dimensionalized to give

$$(A_2/A_1) = \exp\left\{-\frac{1}{4}\int_{G_1^*}^{G_2^*} \alpha_i dG^*\right\}. \tag{12}$$

The expression above is an estimate of disturbance amplitude growth with G^* because the disturbance eigenfunctions change with G^* along a path of constant physical frequency. To assess exactly the growth of a disturbance

one might consider a given disturbance as a starting condition for an initial value analysis. This may require the numerical integration of the full equations in G^*.

The integration in (12) is carried out along the path a disturbance follows across the amplification rate contours as it is convected downstream. The physical frequency ($\tilde{f}$) of a small (linear) disturbance remains constant as it travels. Because of the non-dimensionalization, β decreases proportional to $G^{*-\frac{1}{2}}$. The waves, therefore, travel on paths defined by $\beta . G^{*\frac{1}{2}} = \text{const.}$ The integration was carried out graphically along a family of ten of these curves (three of which are shown in figure 1, $\tilde{f}_1, \tilde{f}_2$ and $\tilde{f}_3$) to give the relative amplification at each point along each of the paths. This information was plotted in the form of amplitude ratio contours (figure 2). The number on a contour is the amplitude

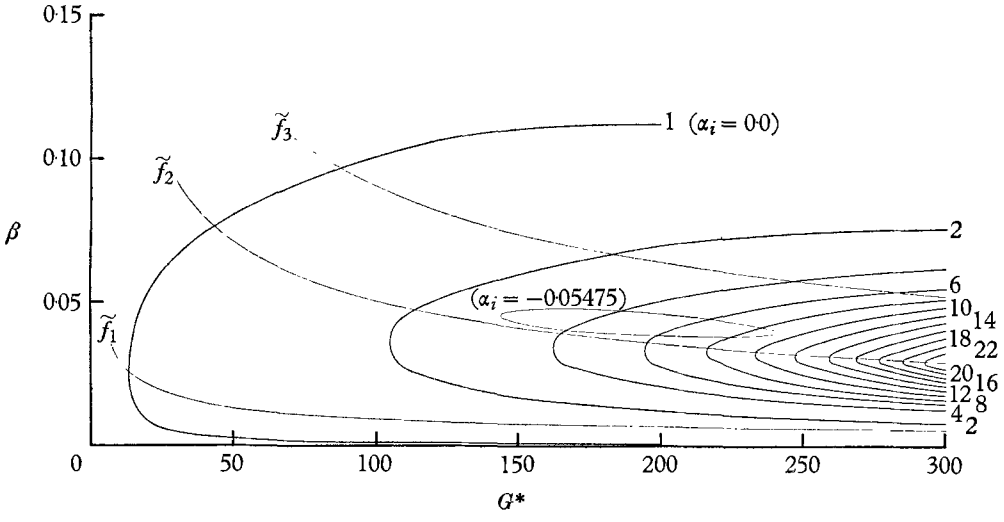

FIGURE 2. Amplitude ratio contours plotted on β-G* co-ordinates.

(non-dimensionalized) a wave will have as it crosses that contour if it had an amplitude of one when it crossed the neutral curve. The maximum amplitude ratio in the range calculated is about 24 at $G^* = 300$ and $\beta = 0{\cdot}029$. The $\beta . G^{*\frac{1}{2}} = \text{const.}$ curve passing through this point is one of the paths shown in figures 1 and 2 ($\tilde{f}_2$). This represents the path of the most amplified frequency, up to $G^* = 300$. This 'most amplified' path depends on the G^*, i.e. downstream location, one is considering. The most amplified path at $G^* = 105$ passes through the point where $\beta = 0{\cdot}035$, which is below the most amplified path for $G^* = 300$ (i.e. $\tilde{f}_2$). The disturbance which begins to amplify first (i.e. at the lowest G^*) is the one whose frequency path passes through the nose of the neutral curve. This disturbance ($\tilde{f}_1$) begins to amplify at the critical G^* (13·5), but when it reaches $G^* = 300$, it has amplified by less than a factor of two. This disturbance begins to amplify first, but since the amplification rates it has are very small, the total amplification at $G^* = 300$ is much less than that of a wide band of higher frequency disturbances (e.g. $\tilde{f}_2$ and $\tilde{f}_3$).

The importance of the critical G^* is further diminished by a consideration of the wavelengths ($\tilde{\lambda}$) there. It can be shown that

$$\left(\frac{\tilde{\lambda}}{\tilde{x}}\right) = \frac{10\pi}{\alpha_r G^*}. \tag{13}$$

Using this relation one can show that at $G^* = 13{\cdot}5$, the wavelength of a disturbance on the path passing through the nose of the neutral curve ($\tilde{f}_1$) is 12·5 times the distance to the leading edge ($\tilde{x}$). Even at a G^* of 300, the wavelength on this same path is about 2·5 times the distance to the leading edge. On the most amplified path to $G^* = 300$ ($\tilde{f}_2$) the wavelength is equal to the distance from the leading edge at the neutral curve ($G^* = 43{\cdot}5$) and about $\frac{1}{3}$ the distance to the leading edge at $G^* = 300$. The shorter wavelengths and the larger amplifications associated with the most amplified path suggests that it is more important in the process of wave amplification, toward actual transition, than is the critical G^* and the nose of the neutral curve.

The real and imaginary parts of the wave velocity (C_r and C_i where $C = \beta/\alpha$) have also been calculated at all the points examined. Some of this information has been shown in figure 1. A line has been plotted on which the real part of the wave velocity is equal to the maximum velocity in the base flow profile ($U_{\max}$). The location of this curve is known exactly only where it crosses the amplification rate contours shown. (There is some uncertainty in the exact location of this curve at $G^* = 300$ because points have not been calculated inside the

$$\alpha_i = -0{\cdot}050$$

contour at this G^*. It is, however, known to be above the lower branch of that contour. Its location here has been interpolated from the contours above and below.) Above this line, C_r is less than $U_{\max}$, and there are two 'critical layers' (i.e. where $C_r = U$) in the boundary layer. Below this line, C_r is greater than $U_{\max}$, and there are no critical layers.

Along a wave path ($\beta . G^{*\frac{1}{2}} = \text{const.}$) C_r is found to be nearly constant. For example, along the two highest paths shown in figures 1 and 2 ($\tilde{f}_2$ and $\tilde{f}_3$) C_r varies by less than 3 % from the neutral curve to $G^* = 300$. This indicates that C_r is increasing with $\tilde{x}$ in nearly the same manner as the base flow velocity (i.e. proportional to $\tilde{x}^{\frac{3}{5}}$). Since the physical frequency is constant, this shows that the wavelength of a disturbance increases as $\tilde{x}^{\frac{3}{5}}$. For flow conditions on the (β, G^*) plane below the curve, (i.e. in the region where $C_r > U_{\max}$), C_r was observed to increase to almost twice $U_{\max}$, and above the curve to decrease to about 6 % below $U_{\max}$.

The eigenfunctions were also examined. The complex eigenfunctions were made more meaningful in a physical sense by converting them into disturbance amplitude and phase angle profiles. The amplitude is the absolute value, and the phase angle is the argument of the complex eigenfunctions. This conversion is discussed by Knowles & Gebhart (1968). Profiles were plotted for the tangential disturbance velocity component, and for the disturbance temperature. In plotting, all of the amplitude profiles have been normalized to one at their maxima. The disturbance temperature phase profiles have been terminated at $\eta = 3$ because the disturbance temperature amplitude is essentially zero there.

Amplitude and phase profiles have been plotted for points near the upper two constant frequency paths ($\tilde{f}_2$ and $\tilde{f}_3$) shown in figures 1 and 2. The profiles change very little with G^*, and only those at the neutral curve and at $G^* = 300$ are shown (figures 3 and 4). For the Prandtl number used (6.7), the locations of the base flow velocity maximum (at $\eta = 0{\cdot}75$) and of the inflexion point (at $\eta = 1{\cdot}34$) are shown.

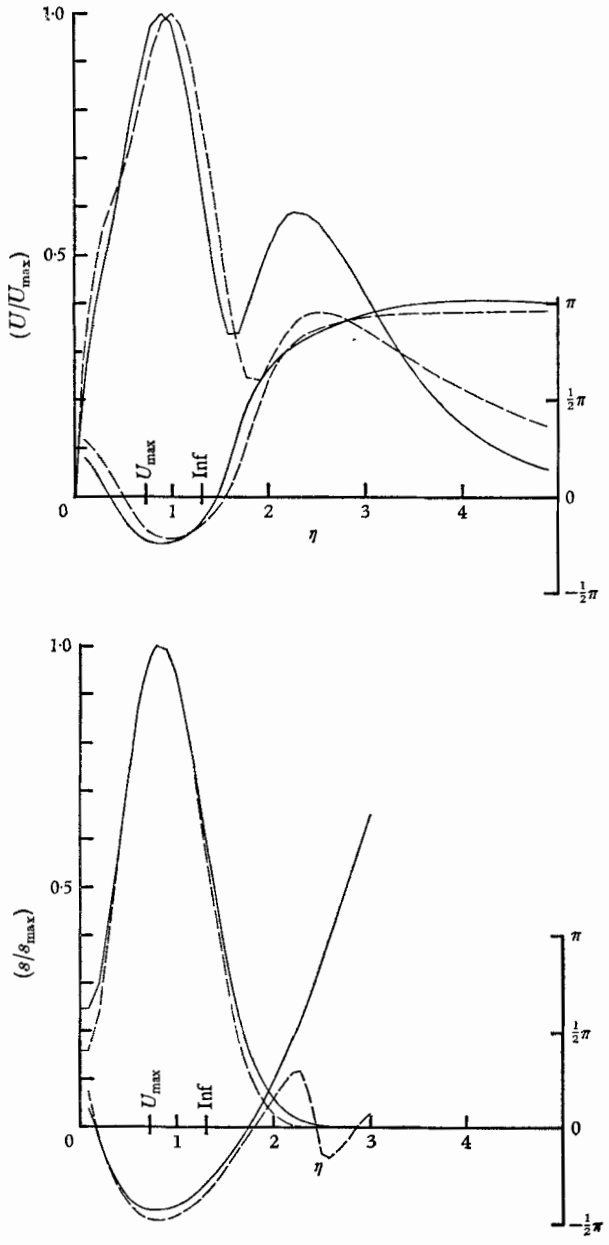

FIGURE 3. Amplitude and phase profiles near $\tilde{f}_3$ at $G^* = 86$, $\beta = 0{\cdot}0961$, $\alpha_i = 0$ (on the neutral curve, solid lines) and at $G^* = 300$, $\beta = 0{\cdot}0518$, $\alpha_i = -0{\cdot}045$ (dashed lines).

As was mentioned earlier, the boundary condition $s'(0) = 0$ is more realistic at small values of G^*, and $s(0) = 0$ is more realistic at large values. The $s'(0) = 0$ condition has, however, been applied over the entire stability plane. In order to demonstrate the effect of this boundary condition, $(s(0)/s_{\max})$ has been plotted against G^* (figure 5) for points along the upper two constant frequency paths ($\tilde{f}_2$ and $\tilde{f}_3$), the upper branch of the neutral curve (U) and part of the lower branch

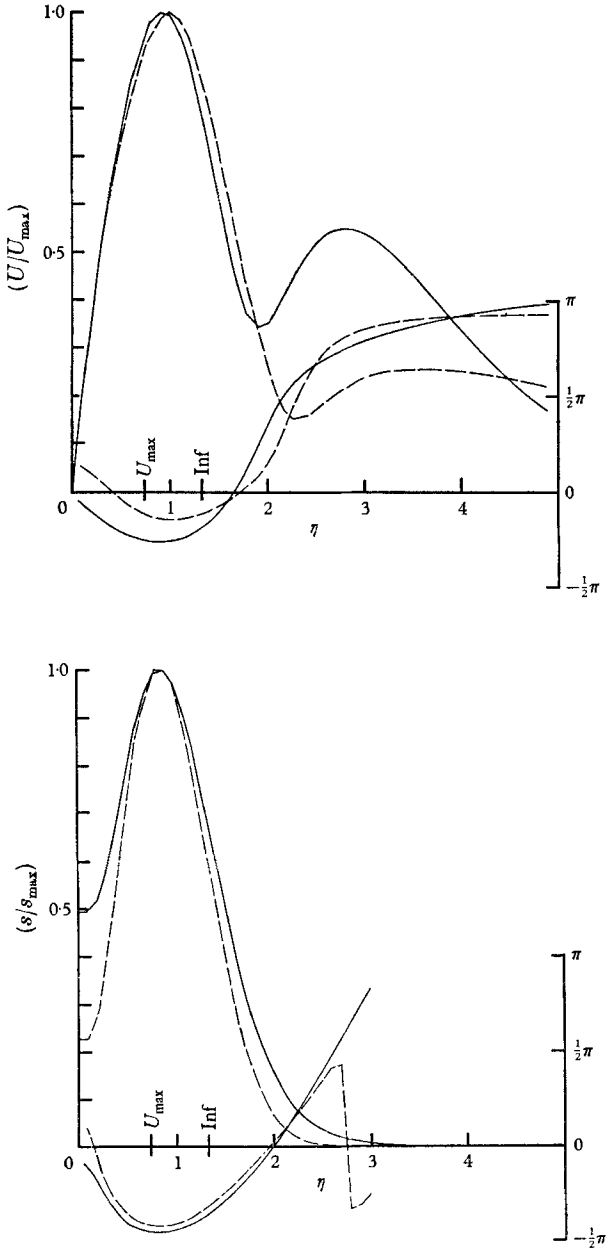

FIGURE 4. Amplitude and phase profiles near $\tilde{f}_2$ at $G^* = 43$, $\beta = 0{\cdot}0760$, $\alpha_i = 0$ (on the neutral curve, solid lines) and at $G^* = 300$, $\beta = 0{\cdot}0295$, $\alpha_i = -0{\cdot}050$ (dashed lines).

(L). Along the neutral curve and along each of the two constant frequency paths ($s(0)/s_{max}$) decreases as G^* increases. This behaviour can also be seen in the disturbance temperature profiles in figures 3 and 4.

The phenomenon of wave amplification in a uniform flux natural convection boundary layer has been under investigation experimentally. The results of this study, which will be published, are in good agreement with the theoretical amplification rates and disturbance profiles presented here.

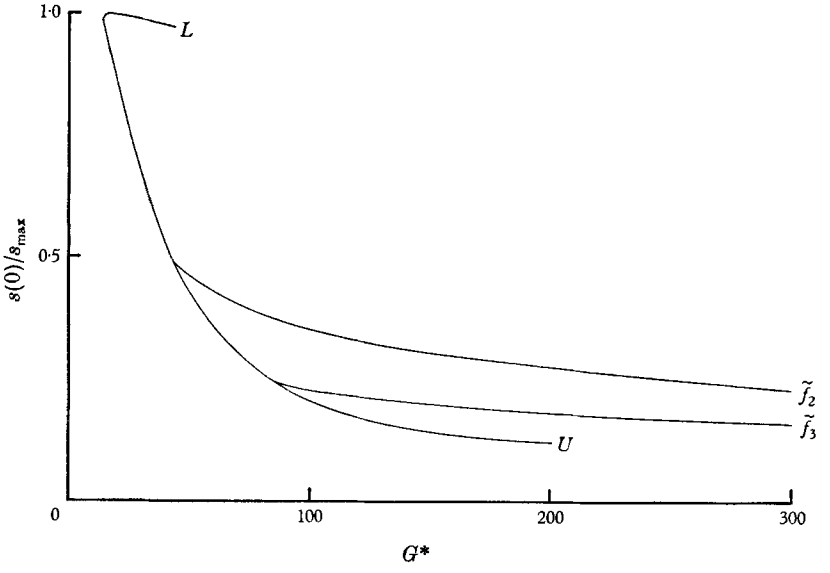

FIGURE 5. ($s(0)/s_{max}$) versus G^*. (U and L correspond to the upper and lower branches of the neutral curve respectively.)

4. Conclusions

The coupled Orr–Sommerfeld equation has been integrated for a Prandtl number of 6·7 and with distance amplification. The $s'(0) = 0$ boundary condition has been applied. It is appropriate for thin surfaces with a very small relative heat capacity. The equations were integrated toward the surface, and the eigenvalues were determined by the Newton–Raphson method used by Nachtsheim (1963). A least-squares eigenvalue extrapolator was used to march in both α_i and G^*. This greatly increased the marching step sizes possible. Employing these techniques the equations were integrated in the damped and amplified regions and up to $G^* = 300$.

There may be some error in the results due to the one-dimensional flow assumption. There is, however, support for such approximation in the good agreement between experimental results of Polymeropoulos & Gebhart (1967) and the theoretical results of Nachtsheim (1963) and of Polymeropoulos & Gebhart (1966) where this assumption is also made. A similar substantiating agreement is indicated by the work of Knowles (1967), in liquids.

The amplification rate contours located in the present work were used to

calculate the relative amplitude of a disturbance as it is convected downstream. The eigenfunctions show how the amplitude and phase profiles of a disturbance vary relatively little as it travels.

A very important result of this investigation was the demonstration that the disturbances which amplify fastest occupy a frequency band which is much higher than the frequency that begins to amplify first. This is not evident from consideration of the neutral curves alone. Amplification is determined by integrating along the paths disturbances follow across the amplification rate contours of the β-G^* diagram as they are convected downstream. The amplitude ratio contours thus produced clearly indicate the most rapidly amplifying band of frequencies. It is this band which one would expect to lead to transition and turbulence. The importance of the critical G^* (and of the frequencies in that region which begin to amplify first) is further diminished when one examines the wavelengths of these disturbances. Over the entire region considered, these wavelengths were much longer than the distance to the leading edge.

We would like to thank Professor S. F. Shen and Dr C. P. Knowles for their many valuable suggestions, and to acknowledge the support of the National Science Foundation, through grants GP-127 and GK-1963 for this research.

REFERENCES

KAPLAN, R. E. 1964 *M.I.T., ASRL TR* 116–1.

KNOWLES, C. P. 1967 Ph.D. Thesis, Cornell University.

KNOWLES, C. P. & GEBHART, B. 1968 Submitted to *J. Fluid Mech.*

NACHTSHEIM, P. R. 1963 *NASA TN-D*-2089.

PLAPP, J. E. 1957 Ph.D. Thesis, Cal. Inst. of Tech.

POLYMEROPOULOS, C. E. & GEBHART, B. 1966 *AIAA J.* **4**, 2066.

POLYMEROPOULOS, C. E. & GEBHART, B. 1967 *J. Fluid Mech.* **30**, 225.

SMITH, A. M. O. 1956 *9th Int. Cong. of Appl. Mech.* **4**, 234.

SPARROW, E. M. & GREGG, J. L. 1956 *ASME Trans.* **78**, 435.